

# Orbital and physical parameters of eclipsing binaries from the All-Sky Automated Survey catalogue – I. A sample of systems with components' masses between 1 and 2 $M_{\odot}$

K. G. Helminiak,<sup>1\*</sup> M. Konacki,<sup>1,2</sup> M. Ratajczak<sup>1</sup> and M. W. Muterspaugh<sup>3,4</sup>

<sup>1</sup>Nicolaus Copernicus Astronomical Center, Department of Astrophysics, ul. Rzybińska 8, 87-100 Toruń, Poland

<sup>2</sup>Astronomical Observatory, A. Mickiewicz University, ul. Słoneczna 36, 60-286 Poznań, Poland

<sup>3</sup>Department of Mathematics and Physics, College of Arts and Sciences, Tennessee State University, Boswell Science Hall, Nashville, TN 37209, USA

<sup>4</sup>Tennessee State University, Center of Excellence in Information Systems, 3500 John A. Merritt Blvd., Box No. 9501, Nashville, TN 37203-3401, USA

Accepted 2009 August 6. Received 2009 July 30; in original form 2009 June 26

## ABSTRACT

We derive the absolute physical and orbital parameters for a sample of 18 detached eclipsing binaries from the All-Sky Automated Survey (ASAS) data base based on the available photometry and our own radial velocity (RV) measurements. The RVs are computed using spectra we collected with the 3.9-m Anglo-Australian Telescope (AAT) and its University College London Echelle Spectrograph (UCLES), and the 1.9-m Radcliffe telescope and its Grating Instrument for Radiation Analysis with a Fibre-Fed Echelle (GIRAFFE) at the South African Astronomical Observatory (SAAO). In order to obtain as precise RVs as possible, most of the systems were observed with an iodine cell available at the AAT/UCLES and/or analysed using the two-dimensional cross-correlation technique (TODCOR). The RVs were measured with TODCOR using synthetic template spectra as references. However, for two objects we used our own approach to the tomographic disentangling of the binary spectra to provide observed template spectra for the RV measurements and to improve the RV precision even more. For one of these binaries, AI Phe, we were able to obtain an orbital solution with an RV rms of 62 and 24  $\text{m s}^{-1}$  for the primary and secondary, respectively. For this system, the precision in  $M \sin^3 i$  is 0.08 per cent.

For the analysis, we used the photometry available in the ASAS data base. We combined the RV and light curves using PHOEBE and JKTEBOP codes to obtain the absolute physical parameters of the systems. Having precise RVs, we were able to reach  $\sim 0.2$  per cent precision (or better) in masses in several cases but in radii, due to the limited precision of the ASAS photometry, we were able to reach a precision of only 1 per cent in one case and 3–5 per cent in a few more cases. For the majority of our objects, the orbital and physical analysis is presented for the first time.

**Key words:** techniques: radial velocities – binaries: eclipsing – binaries: spectroscopic – stars: fundamental parameters.

## 1 INTRODUCTION

The importance of eclipsing binaries for modern astrophysics cannot be underestimated. Their favourable geometry enables one to measure many basic physical parameters of the components, like masses, radii or luminosities which are crucial for our still not complete understanding of stellar evolution. Eclipsing binaries with components in various evolutionary stages work as benchmarks for theory of evolution, distance indication, chemical and dynamical history of the Galaxy. Also a hot topic in modern astronomy –

exoplanets – relies on the knowledge of the host star, its mass and radius. Large, automated, photometric surveys open new possibilities in eclipsing binaries' characterization. Thousands of light curves of eclipsing binaries are being produced for which  $\sim 10 \text{ m s}^{-1}$  and better radial velocity (RV) precision can be obtained (Konacki 2009), and enable one to derive stellar parameters with a precision easily below 1.0 per cent. In particular, the precision in masses may reach 0.01–0.1 per cent level.

In this paper, we present the first results of our ongoing spectroscopic survey of the eclipsing binaries from the All-Sky Automated Survey (ASAS) (Pojmański 2002; Paczyński et al. 2006). Our spectroscopic follow-up to provide RVs was carried out with two high-resolution echelle spectrographs: the University College

\*E-mail: xsyiek@ncac.torun.pl

**Table 1.** 18 DEBs from the ASAS data base and our spectroscopic survey. In the ‘telescope/spectrograph’ column, ‘R/G’ denotes ‘Radcliffe/GIRAFFE’ and ‘A/U’ denotes ‘AAT/UCLES’. If the system was not previously known as an eclipsing or spectroscopic binary before ASAS, a ‘yes’ flag is given in the column ‘new?’. If it was, a reference is given.

ASAS ID	Other ID	Telescope/spectrograph	Distance (pc)	<i>V</i> (mag)	<i>J</i> (mag)	<i>H</i> (mag)	<i>K</i> (mag)	Sp.T.	New?
010538–8003.7	CD-80 28	R/G	–	10.10	8.49	8.04	7.83	K2	Yes
010934–4615.9 <sup>a</sup>	AI Phe, HD 6980	A/U	256	8.60	7.30	6.94	6.82	G8	No (1)
014616–0806.8	BD-08 308	A/U	–	10.52	9.43	9.15	9.05	G2	Yes
023631+1208.6	BD+11 359	A/U	–	9.75	8.70	8.51	8.42	F7	Yes
042041–0144.4	HIP 20267	A/U	116	8.70	7.53	7.25	7.19	G3.5	Yes
042724–2756.2 <sup>b</sup>	IDS04234-2810 A	A/U	–	9.89	8.98	8.84	8.71	F6	Yes
053003–7614.9 <sup>a,b</sup>	UX Men, HD 37513	A/U	101	8.23	7.20	6.98	6.92	F7	No (2)
071626+0548.8	TYC 176-2950-1	A/U	–	10.19	8.97	8.65	8.57	G6	Yes
085524–4411.3	CD-43 4765	A/U	–	10.04	9.00	8.80	8.76	F7	Yes
150145–5242.2	HD 132553	A/U	–	9.58	8.46	8.20	8.19	G0	Yes
155259–6637.8	HD 141344	A/U	–	8.99	7.97	7.75	7.69	F7	Yes
155358–5553.4	HD 141857	A/U	–	9.56	8.45	8.28	8.15	G0	Yes
162637–5042.8 <sup>b</sup>	HD 147827	A/U	–	9.81	8.69	8.44	8.37	G1	Yes
174626–1153.0	BD-11 4457	R/G	–	10.81	8.59	8.16	8.07	K4.5	Yes
185512–0333.8	HD 175375	A/U	–	10.16	9.12	8.97	8.92	F6	Yes
193044+1340.3	V415 Aql, HD 231630	A/U	910	10.41	9.55	9.27	9.18	F6	No (3)
195113–2030.2	HD 187533	A/U	–	9.77	8.63	8.41	8.34	G1	Yes
213429–0704.6	BD-07 5586	A/U	–	10.53	9.47	9.24	9.15	G0	Yes

<sup>a</sup>Photometry is available from ASAS but the star is not indicated as a variable.

<sup>b</sup>Star has a visual and/or physical companion.

*Note.* The available distances are based on the *Hipparcos* parallaxes (Perryman et al. 1997), except for V415 Aql (Branczewicz & Dworak 1980). *V* is the maximum magnitude from ASAS, *J*, *H* and *K* are taken from 2MASS (Cutri et al. 2003). The spectral type is based on  $T_{\text{eff}}$  versus  $V - K$  relation for dwarfs by Tokunaga (2000).

References: (1) Andersen et al. 1988; (2) Andersen et al. 1989; (3) Branczewicz & Dworak 1980.

London Echelle Spectrograph (UCLES) at the 3.9-m Anglo-Australian Telescope (AAT) and the Grating Instrument for Radiation Analysis with a Fibre Fed Echelle (GIRAFFE) at the 1.9-m SAAO Radcliffe telescope. At the AAT/UCLES, we were able to use the iodine cell to improve the RV precision and, in consequence, the precision in masses of the binary stars’ components down to a level better than 0.5 per cent. The available ASAS photometry, when combined with our RVs, enables us to obtain binary star models parametrized with the absolute values of their orbital and physical parameters. The spectroscopic observations, data reduction and the best-fitting orbital/physical solutions for 18 detached eclipsing binaries (DEBs) from the ASAS data base are described below.

## 2 OBJECTS

The targets of this spectroscopic survey are detached spectroscopic binaries with spectral types later than  $\sim F5$  for which precise RV measurements can be made. In order to select the appropriate targets, we proceeded as follows. The ASAS catalogue of variable stars (ACVS; Pojmański 2002) was searched for DEBs with no obvious out-of-eclipse variations, possibly short-lasting eclipses and with  $V - K > 1.1$ . There are 16 such stars in this paper. Two other systems ASAS J010538–8003.7 ( $V - K = 2.27$ ) and ASAS J174626–1153.0 ( $V - K = 2.74$ ) are from our separate observing programme. In order to select relatively bright objects and limit the exposure times but to still have a relatively large sample, we searched for binaries with  $V \leq 11$  mag.

In Table 1, we present the basic characteristics of the targets discussed below. 15 stars turned out to be new variables whose eclipsing nature was first reported in the ACVS. All the systems have their ASAS photometry available online.<sup>1</sup> The time-span of

the ASAS photometry exceeds 8 years, hence a good phase coverage and accurate period determination may be expected. However, the two brightest targets in our sample are not indicated in the ACVS as variables. These are AI Phe (ASAS J010934–4615.9) and UX Men (ASAS J053003–7614.9) previously characterized by Andersen et al. (1988) and Andersen, Clausen & Magain (1989), respectively. For AI Phe, our novel implementation of the iodine cell technique for spectroscopic binaries (Konacki 2009) allows us to improve its parameters, especially masses, to an unprecedented level of precision. For UX Men, we have also obtained a higher precision in masses even though this system has wider spectral lines than AI Phe which reduces the attainable RV precision. We have also substantially improved the characteristics of the third of the previously known eclipsing binaries in this sample – V415 Aql (ASAS J193044+1340.3; Branczewicz & Dworak 1980) – which until now was reported to have two times shorter period, a large brightness ratio and no secondary eclipse.

## 3 OBSERVATIONS

### 3.1 Radcliffe/GIRAFFE

Spectra of the systems ASAS J010538 and ASAS J174626 were obtained during two runs in 2006 June (ASAS J010538) and October (ASAS J174626) with the 1.9-m Radcliffe telescope and GIRAFFE as a part of our low-mass eclipsing binaries search programme. GIRAFFE provides spectra with a resolution of  $\sim 40\,000$ . Due to a relatively low throughput of the entire system, we used the exposure time of 3600 s. The resulting signal-to-noise ratio (SNR) per collapsed spectral pixel varied, and depending on the observing conditions was  $\sim 35$ – $70$  for both the objects. The wavelength calibration was done in a standard manner with a ThAr lamp exposure taken before and after a stellar exposure.

<sup>1</sup> <http://www.astrouw.edu.pl/asas/?page=main>

### 3.2 AAT/UCLES

The rest of the objects were observed with the AAT/UCLES during three runs (11 nights) between 2008 September and 2009 January. We used a 1 arcsec slit which provides a resolution of  $\sim 60\,000$ . Most of the time we adopted an exposure time of 900 s. In good seeing conditions, we were able to obtain an SNR  $\sim 90$  for our typical target and an exposure without the iodine cell. However, usually the SNR was between 30 and 65. In bad seeing conditions, we obtained an SNR  $\sim 30$ –40 for the brightest targets and no iodine cell in the light path. If weather permitted, we used an iodine cell. The exposures with the iodine cell had an SNR about 30 per cent lower than without the cell. The ThAr lamp exposures were also taken throughout each night but not after every single stellar exposure.

An iodine cell becomes useful when an SNR is  $\sim 50$  or more. However, spectra with an SNR as low as  $\sim 30$  taken through an iodine cell can still be reduced. For most of the nights at the AAT, we had to deal with large (above 2 arcsec) and variable seeing, and it was not always possible to decide beforehand if it was practical to use the iodine cell for a given target. In consequence, we ended up with a number of exposures taken through the iodine cell with an SNR too low for high-RV precision. Fortunately, since the iodine cell approach for binary stars always requires taking pairs of exposures with and without the cell (Konacki 2005; Konacki 2009), if we could not use or take an exposure with the cell we always had one without the cell for each target. These were subsequently used to measure an RV with the usual ThAr-based approach. In consequence, we have three types of RV data sets – based entirely on the iodine cell, entirely on the ThAr wavelength calibration or mixed sets when both types of calibrations are used to provide RVs.

## 4 ANALYSIS

### 4.1 Radial velocities

The raw CCD frames taken on both telescopes/spectrographs were reduced in a standard manner (bias subtraction, flat-fielding) with IRAF package CCDRED.<sup>2</sup> The subsequent echelle data reduction was also carried out with IRAF and its ECHELLE package. The RVs from the ThAr-wavelength-calibrated spectra were calculated with our own implementation of the two-dimensional cross-correlation technique (TODCOR; Zucker & Mazeh 1994). As templates, we used synthetic spectra computed with the ATLAS9 and ATLAS12 codes (Kurucz 1992). With the exception of two systems, AI Phe (ASAS J010934) and UX Men (ASAS J053003), the RVs from the iodine-cell-calibrated spectra were also computed with TODCOR. The details of such a procedure are described by Konacki (2005).

For the two brightest binaries in this sample, UX Men (ASAS J053003) and AI Phe (ASAS J010934), we were able to collect eight spectra taken with the iodine cell each. This is about the smallest number of spectra still sufficient to carry out a tomographic disentangling to obtain observed component spectra of a binary. Our disentangling procedure is described by Konacki (2009). It essentially allows one to derive the component spectra from the observed composite spectra and then use them to compute the RVs. As we

have shown, this approach is capable of providing RVs of the components of double-line binary stars with a precision reaching  $5\text{ m s}^{-1}$  (Konacki 2009). While the spectra of UX Men and AI Phe from the AAT/UCLES are characterized by a much lower SNR of  $\sim 40$ –100 compared to those used in Konacki (2009), the disentangling still can be carried out. This procedure has resulted in a higher RV precision compared to the standard ThAr approach or the iodine-cell-based approach combined with TODCOR for these two targets. In particular, the best-fitting RV solution for AI Phe is characterized by an rms of 62 and  $24\text{ m s}^{-1}$  for the primary and secondary, respectively. The UX Men rms is not nearly as good (210 and  $270\text{ m s}^{-1}$ ), but this is due to the very wide spectral lines of its components. There is no doubt that the RV precision for AI Phe would be much higher if higher SNR spectra were available. It should be noted here that the RV precision from the iodine-cell spectra used in this paper is not representative for this technique as most of the time we were dealing with an SNR far too low for what is required to obtain a high RV precision. Still the results are quite satisfactory precision wise.

For seven systems, the iodine-cell-based solution was substantially better than the ThAr-based one. For four other targets, we used RVs based on both methods of wavelength calibration since the number of iodine-cell-based spectra was too small or the resulting rms was comparable. The seven remaining targets (including the two observed at SAAO) have their solutions based on the ThAr-calibrated spectra only.

The RV measurements together with their errors and O – C are collected in Table A1 in Appendix A. As it turned out the formal errors  $\sigma_0$  computed from the scatter between the echelle orders used in the analysis were somewhat underestimated. Hence, to obtain  $\chi^2 \simeq 1$  for our RV solutions and more conservative estimates of the errors of the best-fitting orbital and physical parameters, we added in quadrature an additional error  $\sigma_{\text{sys}}$  to the formal RV errors. For every component of every binary, the additional RV error was estimated independently and in general varied from star to star. There are a few possible sources of such errors. For the ThAr-based RVs, the largest additional contribution to the error budget comes from a wavelength solution based on ThAr taken sometime before or after a stellar exposure and hence usually not just before or after. For the iodine-cell-based RVs, most likely the additional RV error comes from an imperfect modelling of the spectrograph’s point spread function imposed by a relatively low SNR of the spectra. Presumably, also the intrinsic RV variability of the stars itself contributes to the error budget. In Table A1, final RV errors are shown.

### 4.2 Modelling

Our RV measurements were combined with the available ASAS photometry to derive absolute physical and orbital parameters of our targets. We used three independent modelling codes, each of them for a different purpose, as follows.

First of all, we used the light curve modelling code JKTEBOP (Southworth, Maxted & Smalley 2004a; Southworth et al. 2004b) based on Eclipsing Binary Orbit Program (EBOP; Etzel 1981; Popper & Etzel 1981), which fits a simple geometric model of a DEB to a single light curve. We obtained preliminary yet quite accurate values of the orbital period  $P$  and the moment  $T_0$ . A preliminary value of the mass ratio was assumed (usually close to or equal 1) in this step.

Secondly, we derived the orbital parameters using the RV measurements only. For that purpose, we used our own software which fits a Keplerian orbit by minimizing the  $\chi^2$  function with the

<sup>2</sup> IRAF is written and supported by the IRAF programming group at the National Optical Astronomy Observatories (NOAO) in Tucson, AZ. NOAO is operated by the Association of Universities for Research in Astronomy, Inc. under cooperative agreement with the National Science Foundation. <http://iraf.noao.edu/>

least-squares Levenberg–Marquardt algorithm. With this software, for a circular orbit, we fit for a zero phase (time of periastron for an eccentric orbit), two RV amplitudes and systemic velocity. For an eccentric orbit, we also fit for an eccentricity and longitude of periastron. The fit is performed simultaneously to the RVs of both stars as, by definition, their longitudes of periastron differ by  $180^\circ$ , but otherwise the stars follow the same orbit. This way from, for example, five visits to a binary we have 10 RV measurements and four (circular orbit) or six (eccentric orbit) parameters to fit for. We held the orbital period fixed at the value taken from JKTEBOP. The choice of a circular or eccentric RV orbit was based on a light curve only. This way, we obtained precise values of the orbital/physical parameters related to RVs, especially the mass ratio  $q$  from the RV amplitudes  $K_{1,2}$ , which were later used in the next JKTEBOP runs. After the second JKTEBOP run, we obtained improved values of  $T_0$  and  $P$  which were finally used with the third code – Physics Of Eclipsing Binaries (PHOEBE; Prša & Zwitter 2005), an implementation of the Wilson–Devinney (WD) code (with updates Wilson & Devinney 1971).

PHOEBE allows one to fit a model to the RV and light curves simultaneously. We used it to create the final model of each binary. Our criterion for a best-fitting solution is a model given by PHOEBE which is also in agreement with the other two codes. However, the uncertainties given by PHOEBE tend to be underestimated, so for the error estimations we used our RV-fitting code and JKTEBOP code that employs a Monte Carlo simulator.

Binaries with eccentric orbits happen to cause a few problems when analysed in the way described. The main issue is the fact that every code defines its zero moment  $T_0$  in a different way. In our RV-fitting code,  $T_0$  is the periastron passage. JKTEBOP defines  $T_0$  as the moment of the deeper eclipse which is then called *primary* (eclipse of the *primary* star). In PHOEBE,  $T_0$  corresponds to the far intersection between the projection of the line of sight through the centre of the ellipse on the orbital plane and the ellipse (Prša 2006). The primary eclipse in general *does not* coincide with  $T_0$  and is defined as the one closer to  $T_0$ . This convention is useful when an apsidal motion is present. In such a case, no artificial period change is seen (as it is when  $T_0$  is fixed to an eclipse). We decided to keep the convention from PHOEBE but to force the *deeper* eclipse to be closer to  $T_0$ . Hence, we call the *primary* the star whose eclipse is the deeper one.

The initial values of the eccentricity  $e$  and the periastron longitude  $\omega$  were calculated with JKTEBOP. Later, the values of  $e$  and  $\omega$  were improved with our RV-fitting code. In the two eccentric orbit cases when we only had three spectra and thus the number of RV measurements was only six,  $e$  and  $\omega$  were not fitted with the RV code. The same was done for ASAS J014616 and ASAS J071626, despite having actually five measurements, as some of them (with and without  $I_2$ ) were made during the same night one after another. The final values of  $e$  and  $\omega$  were determined with PHOEBE. This code is not particularly efficient in fitting for  $e$  and  $\omega$ , so we typically restarted it with slightly different values of  $e$  and  $\omega$  to match the difference in phase between the light curve’s two minima as determined by JKTEBOP. Due to the different definitions of  $T_0$ , in some cases we had to change the initial value of  $\omega$  by  $180^\circ$ . The final set of the orbital parameters and the O – C for the RVs and ASAS photometry are all in the framework of PHOEBE.

## 5 RESULTS

The results of our modelling of 18 DEBs are shown in Table 2. The orbital and physical parameters are given with their  $1\sigma$  uncertainties.

We show the basic parameters that are computed directly with the codes used or can be computed as a combination of the directly determined values. We do not present bolometric magnitudes and luminosities nor separate effective temperatures. The temperatures may be computed with PHOEBE but are highly dependent on their starting values. However, the temperature ratio is considered to be reliable (Prša 2006), and it is shown in the last column of Table 2. All our solutions are presented in Fig. 1. It should be noted that the reference phase ( $\phi = 0$ ) is defined as in PHOEBE. For eccentric orbits, it means that this does not coincide with minima. For the purpose of ephemeris calculations and a possible further eclipse timing, in Table 3 we show the phases of the primary and secondary minima for eight eccentric systems in our sample.

### 5.1 Masses, radii and its uncertainties

For five of our targets, the relative errors in masses,  $\Delta M/M$ , are higher than 1 per cent. These include the two systems observed with Radcliffe/GIRAFFE – ASAS J010538 (4 per cent for both components) and ASAS J174626. (1.8 and 2.2 per cent for the primary and secondary, respectively) and three from AAT/UCLES data – ASAS J014616 (1.9 and 2.0 per cent), ASAS J150145 (1.2 per cent for both) and ASAS J213429 (2.7 and 2.9 per cent). For two targets, we reached the error in masses below 0.2 per cent. These are ASAS J053003 (UX Men, 0.164 and 0.168 per cent) and ASAS J010934 (AI Phe) for which we reached 0.091 and 0.087 per cent precision in the masses of the primary and secondary components, respectively. It is worth noting that UX Men and AI Phe were observed spectroscopically only eight times each. Three other systems with high-mass precisions are ASAS J085524 (0.22 and 0.24 per cent, three ThAr and two iodine-cell-calibrated spectra), ASAS J155259 (0.22 and 0.25 per cent, four iodine-cell-calibrated spectra) and ASAS J155358 (0.32 and 0.31 per cent, four iodine-cell-calibrated spectra). A similar level of precision ( $\sim 0.4$  per cent) in  $M \sin^3 i$  was reported for only few other eclipsing binaries, like AD Boo, VZ Hya and WZ Oph by Clausen et al. (2008), but in these cases the number of RV measurements for each system reached 100. Our results presented in Table 2 also include an uncertainty in the inclination angle. The relative precision of the  $M \sin^3 i$  only is 0.08 per cent for our RV data set of AI Phe.

Contrary to the derived masses, our radii estimations are not as precise. We were using only the available ASAS photometry which on the one hand provides over 8 years of observations and a full phase coverage but on the other hand the total scatter ( $\sim 6\sigma$ ) of ASAS data points often exceeds 0.1 mag. Also, when eclipses are short lasting, occupying a small fraction of the orbital period, the number of single data points during an eclipse is low, often below 20. This issue has its direct impact on the precision of such parameters like the sum and ratio of radii, temperature ratio and the inclination. In the worst case – ASAS J014616 – our precision in radii is about 30 per cent. Seven other systems have their radii measured with uncertainties between 10 and 20 per cent for the primaries and between 10 and 27 per cent for the secondaries. However, on the other side of the scale there are five systems with radii precision equal to or better than 3 per cent. These include ASAS J010934 (AI Phe; 2.7 and 2.5 per cent), ASAS J053003 (UX Men; 2.7 and 2.9 per cent), ASAS J071626 (1.9 and 1.7 per cent), ASAS J085524 (1.1 and 1.0 per cent) and ASAS J193044 (V415 Aql; 3.0 and 2.8 per cent). The results given above could be significantly improved if one had high-precision photometry available.

**Table 2.** Absolute orbital and physical parameters from our solutions for the investigated targets with  $1\sigma$  uncertainties in parentheses.

ASAS ID	Solution	$P$ (d)	$T_0$ (PHOEBE) JD 245 0000	$K_1$ (km s $^{-1}$ )	$K_2$ (km s $^{-1}$ )	$v_{\gamma}$ (km s $^{-1}$ )	$q$	$a$ ( $R_{\odot}$ )
010538–8003.7	ThAr	8.069 406(6)	1873.449(6)	73.6(1.6)	73.3(2.4)	–5.8(7)	1.003(31)	23.4(5)
010934–4615.9	iodine <sup>a</sup>	24.592 41(8)	3247.184(3)	51.16(3)	49.11(2)	–0.750(12)	1.0418(8)	47.855(19)
014616–0806.8	mixed	5.940 047(25)	1878.427(7)	76.2(1.1)	84.2(8)	35.0(6)	0.905(16)	18.79(16)
023631+1208.6	ThAr	3.604 913(8)	2449.258(2)	85.8(4)	102.3(3)	6.2(2)	0.839(7)	13.40(4)
042041–0144.4	iodine	6.476 49(2)	1943.030(6)	74.27(38)	81.48(38)	–17.2(1)	0.911(7)	19.76(7)
042724–2756.2	iodine	8.946 57(5)	1873.707(7)	74.0(4)	70.7(4)	7.79(4)	1.047(8)	25.6(1)
053003–7614.9	iodine <sup>a</sup>	4.181 096(3)	2019.2755(11)	87.31(12)	89.90(8)	48.86(5)	0.9712(16)	14.639(12)
071626+0548.8	mixed	11.554 78(6)	2426.025(8)	61.2(3)	62.1(3)	15.6(3)	0.986(7)	27.5(1)
085524–4411.3	mixed	7.040 274(14)	1875.092(4)	68.0(1)	77.50(12)	21.23(7)	0.8772(19)	20.279(22)
150145–5242.2	iodine	5.976 930(76)	1927.389(7)	89.1(7)	88.9(7)	4.6(7)	1.002(10)	21.01(11)
155259–6637.8	iodine	5.744 754(22)	1931.664(6)	93.47(12)	76.98(6)	11.00(5)	1.214(2)	19.367(15)
155358–5553.4	iodine	5.691 743(23)	1933.457(6)	94.59(5)	90.67(9)	4.83(4)	1.043(1)	20.877(11)
162637–5042.8	ThAr	8.876 21(5)	1939.350(11)	65.67(17)	77.39(35)	–28.5(1)	0.852(2)	25.16(5)
174626–1153.0	ThAr	3.011 055(7)	1956.245(3)	116.2(9)	96.2(1.5)	–57.2(7)	1.21(2)	12.63(11)
185512–0333.8	ThAr	5.795 527(15)	1972.545(4)	80.40(5)	96.37(10)	–17.08(5)	0.834(1)	20.257(13)
193044+1340.3	ThAr	4.925 489(16)	2731.560(4)	91.34(55)	98.0(6)	13.5(5)	0.93(1)	18.44(8)
195113–2030.2	mixed	7.043 35(5)	1976.202(9)	65.41(14)	90.71(21)	–8.1(1)	0.7211(23)	21.873(35)
213429–0704.6	ThAr	5.672 517(8)	1884.2545(25)	75.(2)	79.3(7)	–21.0(7)	0.95(3)	17.24(24)
ASAS ID	$e$	$\omega$ ( $^{\circ}$ )	$i$ ( $^{\circ}$ )	$M_1$ ( $M_{\odot}$ )	$M_2$ ( $M_{\odot}$ )	$R_1$ ( $R_{\odot}$ )	$R_2$ ( $R_{\odot}$ )	$T_2/T_1$
010538–8003.7	0.0	–	80.4(6)	1.380(55)	1.384(55)	3.16(33)	4.06(41)	0.72(3)
010934–4615.9	0.187(4)	110.1(9)	84.4(5)	1.2095(11)	1.2600(11)	1.82(5)	2.81(7)	0.820(15)
014616–0806.8	0.067(45)	100(5)	86.1(7)	1.335(25)	1.208(24)	1.57(53)	1.42(52)	1.014(80)
023631+1208.6	0.0	–	87.4(9)	1.357(8)	1.138(7)	1.82(36)	1.28(29)	0.988(18)
042041–0144.4	0.132(5)	342.2(9)	88.5(3)	1.293(9)	1.179(9)	1.59(29)	1.43(26)	0.99(11)
042724–2756.2	0.012(4)	238(24)	86(1)	1.383(13)	1.449(13)	2.2(1)	2.16(8)	0.94(3)
053003–7614.9	0.0	–	89.86(15)	1.2229(15)	1.1878(15)	1.321(36)	1.285(37)	0.992(18)
071626+0548.8	0.21(5)	52(10)	88.2(7)	1.055(8)	1.041(8)	1.65(3)	1.18(2)	0.988(10)
085524–4411.3	0.0	–	86.4(2)	1.2040(27)	1.0562(25)	1.87(2)	1.634(16)	0.996(6)
150145–5242.2	0.0	–	84.7(3.4)	1.766(21)	1.769(21)	2.86(14)	2.81(14)	1.004(27)
155259–6637.8	0.0	–	84.5(8)	1.352(3)	1.644(4)	1.83(15)	2.81(15)	0.984(35)
155358–5553.4	0.0	–	86.3(9)	1.847(6)	1.927(6)	2.73(28)	2.99(30)	0.97(5)
162637–5042.8	0.019(10)	341(2)	85.6(3)	1.469(8)	1.246(7)	2.55(33)	2.25(33)	0.98(4)
174626–1153.0	0.0	–	81.4(5)	1.44(3)	1.74(3)	1.99(12)	2.64(17)	0.95(3)
185512–0333.8	0.0108(3)	45(2)	87.4(1.4)	1.813(6)	1.513(5)	1.7(3)	1.5(4)	0.87(4)
193044+1340.3	0.0	–	87.6(7)	1.798(16)	1.675(15)	2.97(9)	2.34(8)	0.974(16)
195113–2030.2	0.0	–	83.4(3)	1.646(8)	1.187(6)	2.74(13)	2.03(11)	0.994(18)
213429–0704.6	0.0937(8)	170(10)	89(1)	1.10(3)	1.04(3)	1.27(23)	1.24(22)	0.96(3)

<sup>a</sup>Spectra were tomographically disentangled.

## 5.2 Age estimations

As pointed out by Blake et al. (2008), a 3 per cent level of precision is already suitable for performing reliable tests of the evolutionary models. Among objects from our sample, one may find several that are interesting. In Fig. 2, we have shown all our objects in a mass–radius plane. The components of each binary are connected with a dotted line. For a comparison, we have also plotted four  $Y^2$  isochrones (Yi et al. 2001) for the ages of 2 Myr, 0.1, 1.6 and 5 Gyr and solar metallicity.

We used the full set of  $Y^2$  isochrones of solar metallicity to roughly estimate ages of the investigated systems. The isochrones were fitted by eye to our measurement of masses and radii. As one can see, many systems occupy a region where pre-main-sequence (PMS) isochrones (2 Myr as an example) overlap with older ones (1.6 or 5.0 Gyr). 14 of our systems are in this area and for most of them, it was not straightforward to determine their evolutionary stage in the  $M - R$  plane especially given the fairly large uncertainties in radii. In order to gain more confidence in the

estimated ages, we also verified whether the resulting temperature ratios for a given isochrone are consistent with those determined from the light curves. Still for many of the systems, we could find two isochrones that fit to the system’s parameters. Obviously, the estimated ages should be treated as very preliminary ones.

Three of the binaries seem to fit better to a PMS isochrone – ASAS J042724 (the two solutions are 0.002 and 3.0 Gyr), ASAS J085524 (0.003 and 7.0 Gyr) and ASAS J162637 (0.0015 and 4.0 Gyr). Four other systems, ASAS J174626 (0.002 and 2.0 Gyr), ASAS J193044 (V415 Aql; 0.0015 and 1.5 Gyr), ASAS J195113 (0.0015 and 3.0 Gyr) and ASAS J213429 (0.008 and 6.0 Gyr), also seem to prefer a PMS isochrone, but this is not as clear as for the previous three. The systems ASAS J014616 (0.006 and 3.0 Gyr), ASAS J155259 (0.002 and 2.5 Gyr), ASAS J042041 (0.006 and 4.0 Gyr) and ASAS 155358 (0.0015 and 1.2 Gyr) seem to fit better to the more evolved isochrone. For six other binaries ASAS J010538 (4.0 Gyr), ASAS J010934 (AI Phe; 5.0 Gyr), ASAS J023631 (3.5 Gyr), ASAS J053003 (UX Men; 2.75 Gyr), ASAS J071626

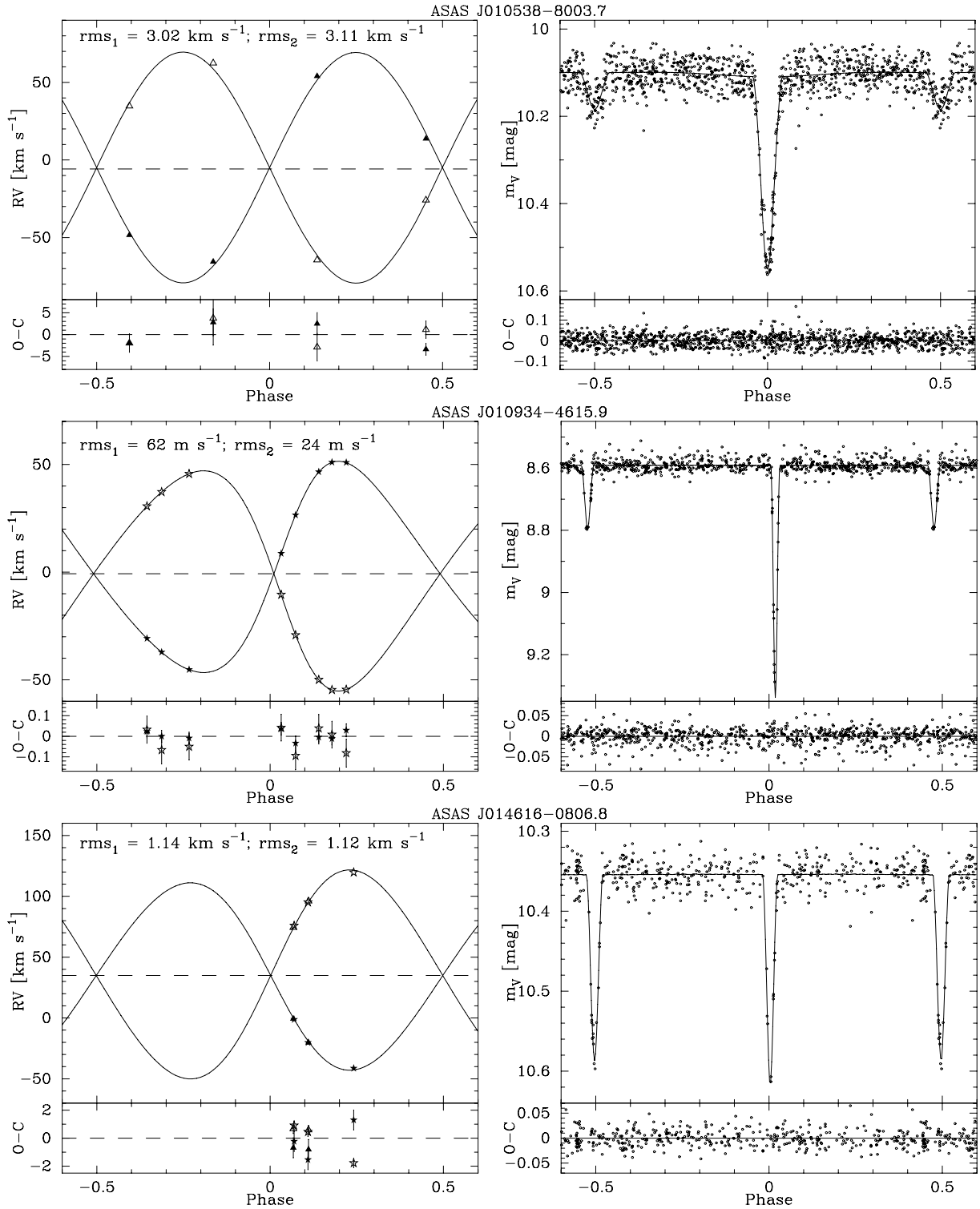


**Figure 1.** Final solutions for all 18 systems. Plots are phase folded with the corresponding periods. Left-hand panels show our RV measurements with the best-fitting solutions. Filled symbols are for the primaries and open ones for the secondaries. Triangles are for the ThAr-calibrated spectra and stars for the iodine-cell-calibrated spectra. The resulting rms and O – C are also shown. Right-hand panels depict the ASAS light curves and our model curves together with O – C.

(8.0 Gyr) and ASAS J185512 (0.4 Gyr), we obtained only one isochrone each consistent with their parameters. The remaining system, ASAS J150145, is composed of nearly twin stars, so to estimate its age one should use other indicators. It is worth noting that

the oldest binary, ASAS J071626 (8 Gyr), despite having relatively short period ( $P \sim 11.5 \text{ d}$ ), has a significantly eccentric orbit ( $e \simeq 0.2$ ). For AI Phe and UX Men, our estimates of the age are close to the literature values (Lastennet & Valls-Gabaud 2002).

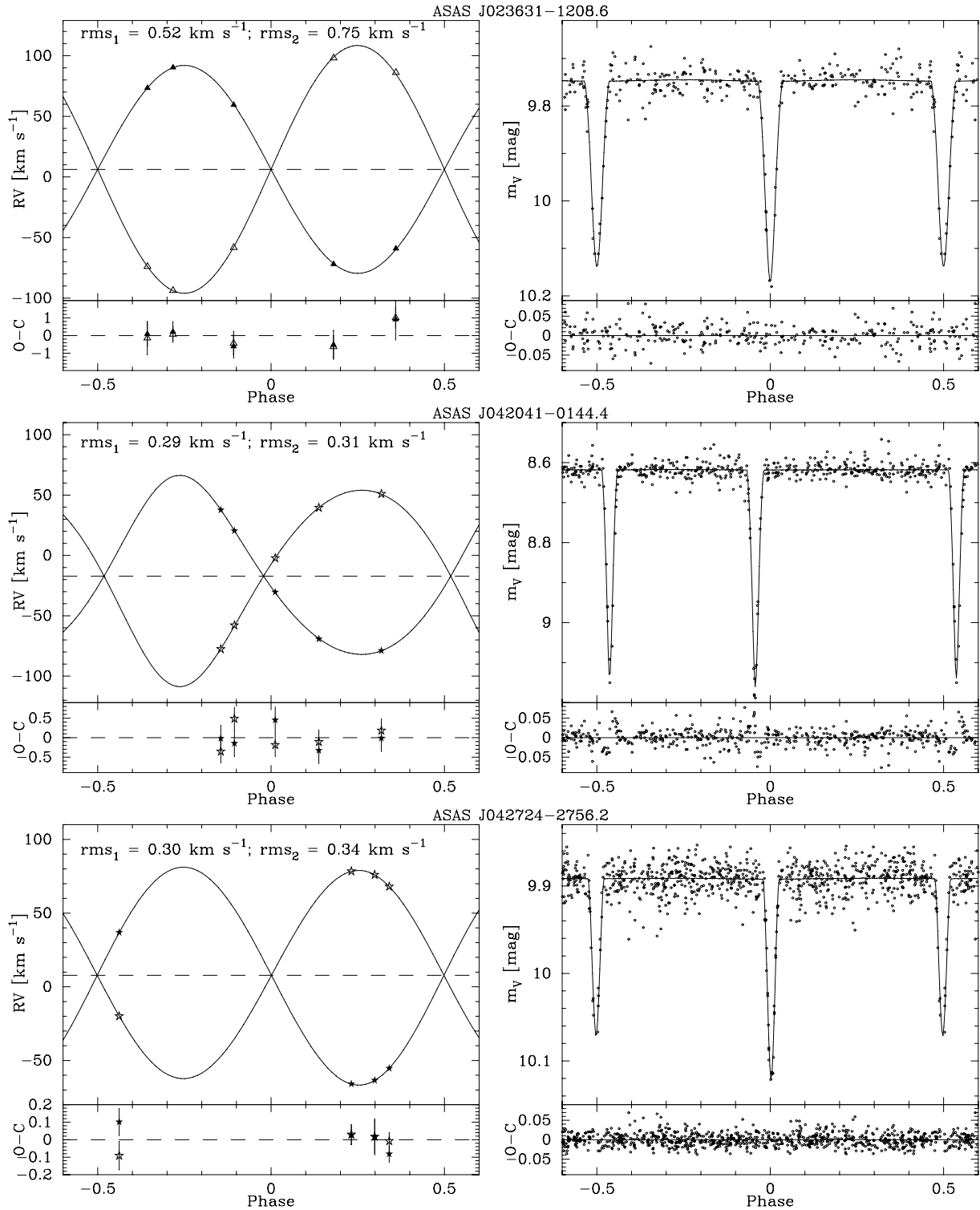


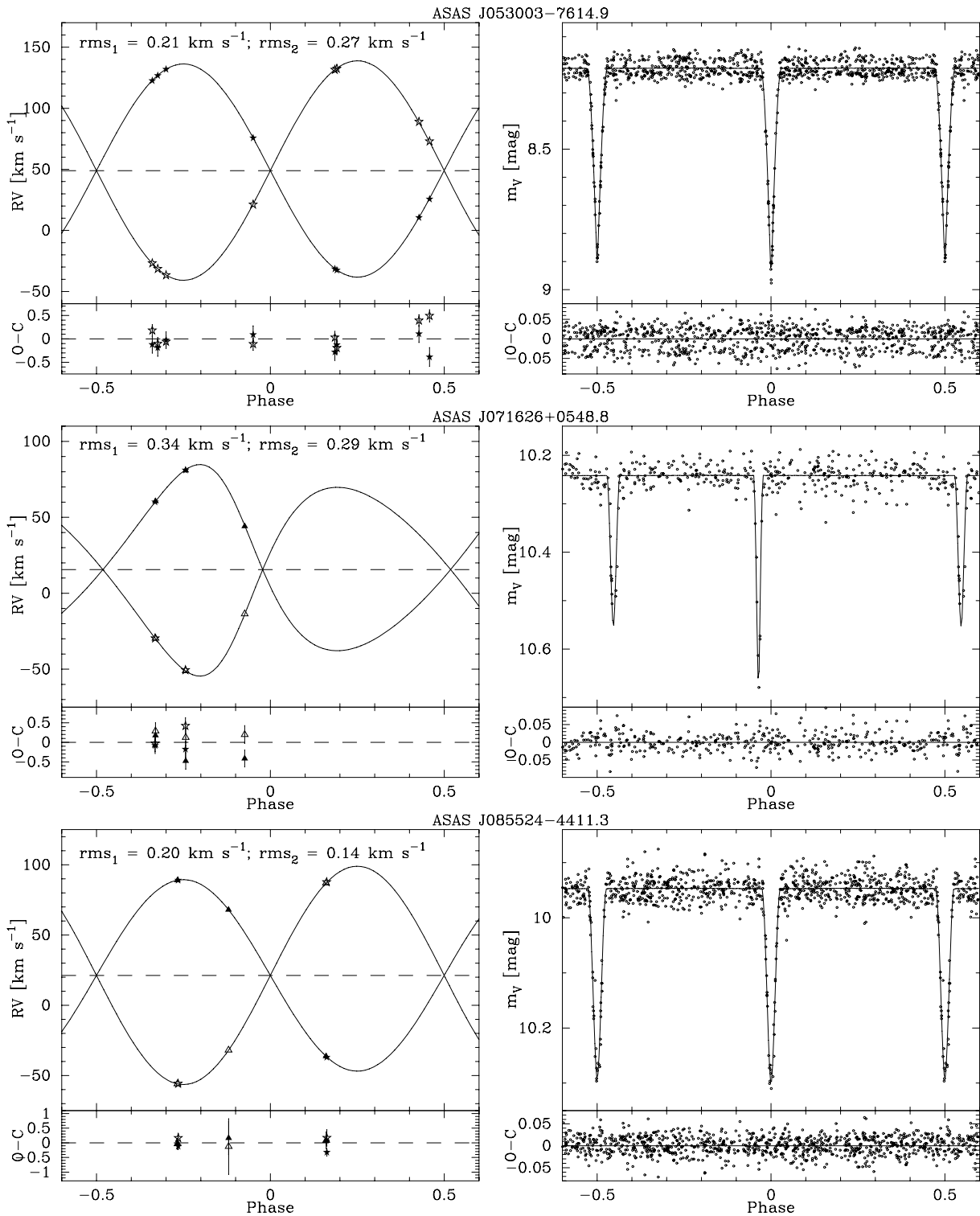
Figure 1 – continued

### 5.3 Comparison with literature

#### 5.3.1 ASAS J010934-4615.9 = *AI Phe*

This system was reported as an eclipsing binary by Strohmeier (1972) and as a double-lined spectroscopic binary by Imbert (1979) who also determined the first orbital solution. This solution was

later improved by Hrivnak & Milone (1984) who used Imbert's RV data and new  $U, B, V, R, I$  photometry to obtain a full set of physical parameters of the system. Later, Andersen et al. (1988) used new CORAVEL RV data together with the unpublished  $u, v, b, y$  light curves and obtained a new model of the system improving parameters' uncertainties by almost an order of magnitude. However, the most up-to-date solution was given later by Milone, Stagg & Kurucz

Figure 1 – *continued*

(1992). They used RV from Andersen et al. (1988), *U, B, V, R, I, u, b, v, y* light curves and far-ultraviolet observations in three bandpasses of the systems' eclipse from Milone et al. (1981) and processed the data with their improved version of the WD code. More recently, a re-analysis of Andersen et al. (1988) RV's was obtained by Karami & Mohebi (2007) with a further improvement of the spectroscopic parameters. However, their solution can be considered as disputable

since they seem not to have included several uncertainties (of the orbital period, for example) into the total error budget and thus presumably underestimated the final errors.

Our solution, based *only* on our RV data and ASAS photometry, is compared with the ones from Andersen et al. (1988) and Milone et al. (1992) in Table 4. In general, our results are in agreement with the previous papers. One should note that having only eight

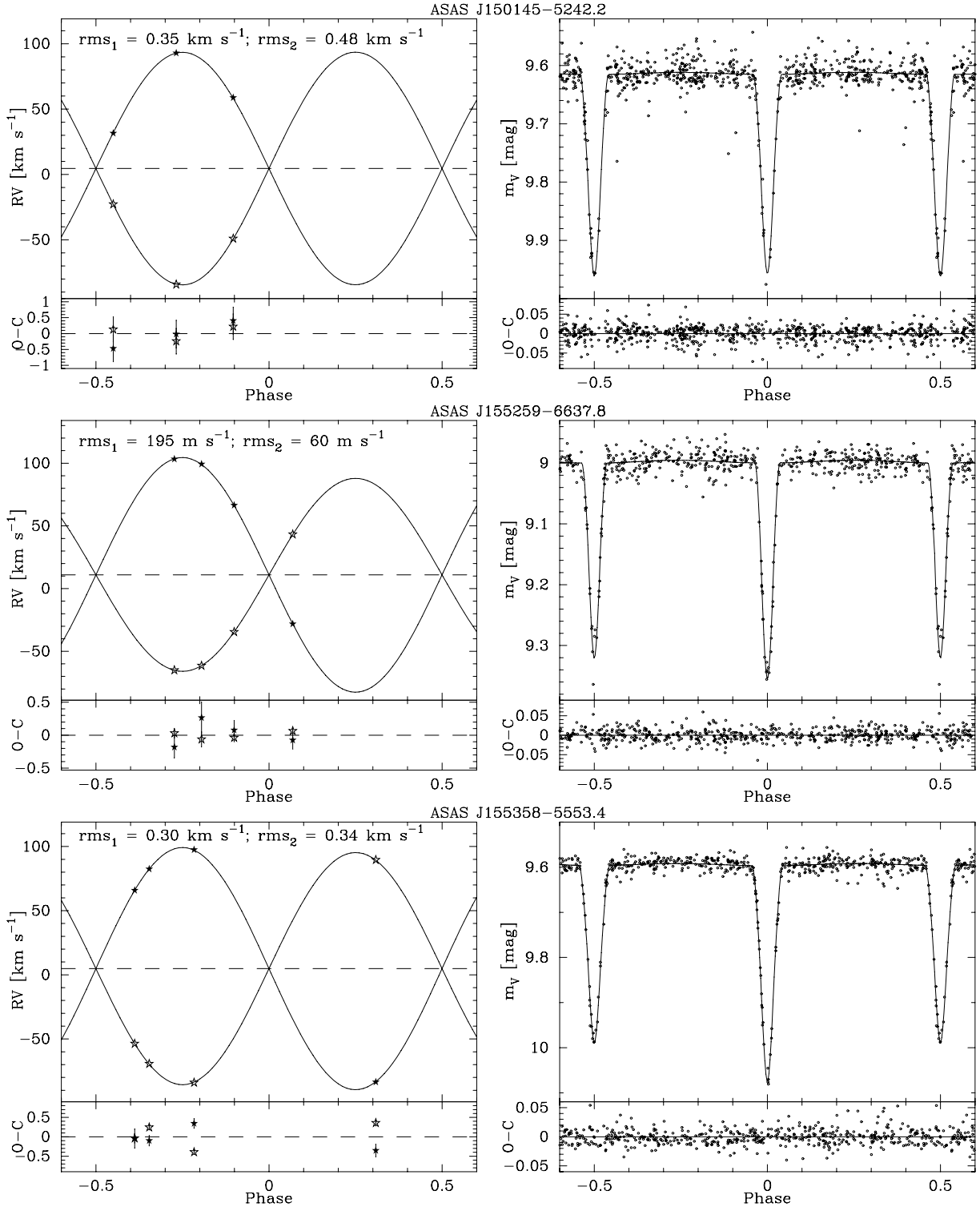
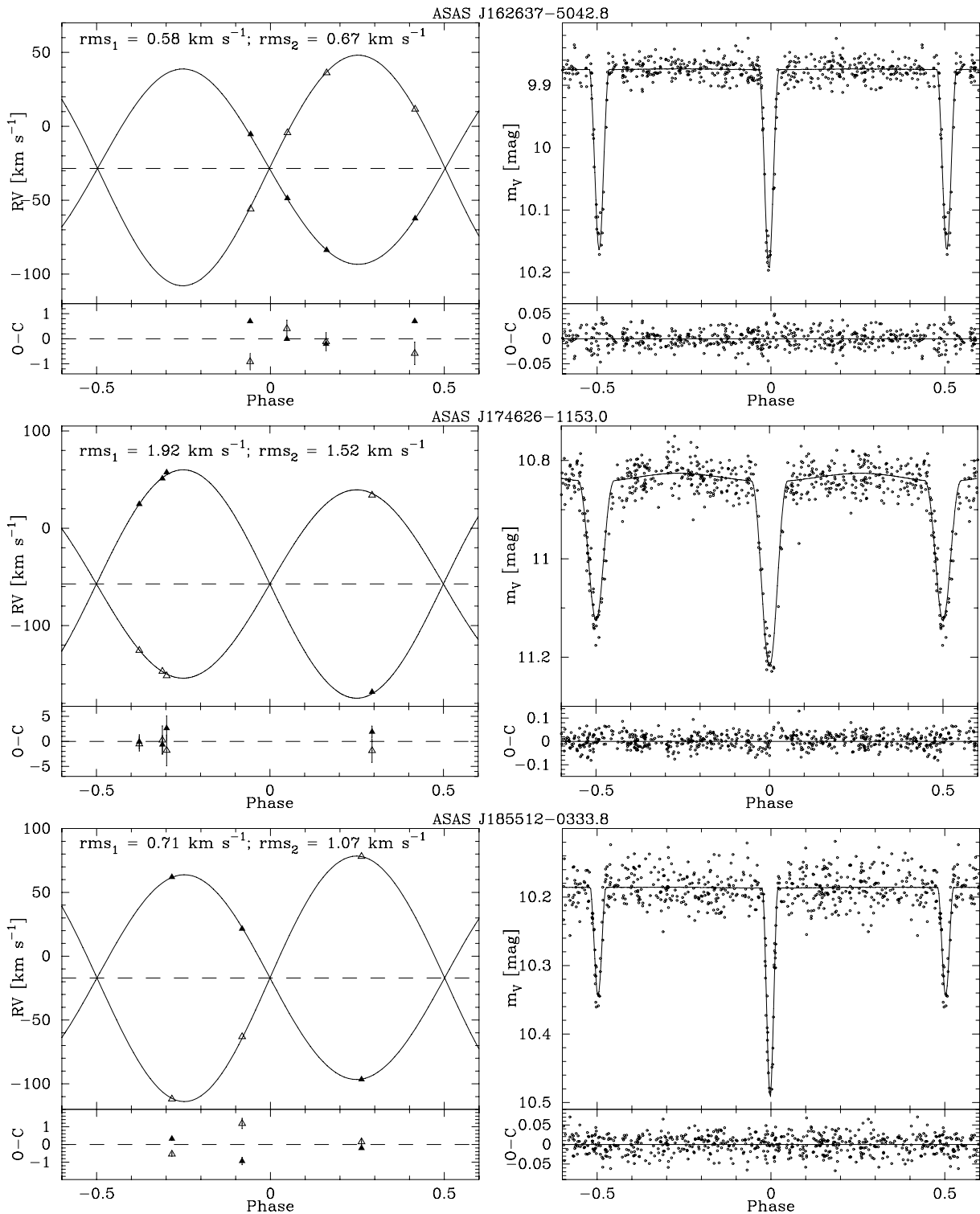


Figure 1 – continued

RV measurements for every component, we were able to improve the spectroscopic results of Andersen et al. (1988), who had 46 data points for every component, by a factor of 2–4. Unfortunately, having only one light curve from ASAS, we cannot compete with the results of Milone et al. (1992) who used light curves from 12 band-passes, most of which were more precise than ours. Still, their phase coverage is not complete and the orbital and physical parameters might be improved with high-precision photometry. Our solution

converged to a somewhat different value of the orbital inclination than Andersen’s and Millone’s. This is of course the reason for the discrepancy in absolute masses between the solutions. Our  $M \sin^3 i$  is however far more precise. Thus, we may conclude that this system’s parameters can be derived with an unprecedented precision (possibly  $\sim 0.01$  per cent in masses and  $\sim 0.1$  per cent in radii) if only one had more iodine RV measurements and millimagnitude photometry.

Figure 1 – *continued*

### 5.3.2 ASAS J053003-7614.9 = UX Men

UX Men, as well as AI Phe, was discovered to be a variable in Bamberg patrol plates and reported by Strohmeier, Fischer & Ott (1966). The first orbital solution was obtained by Imbert (1974) and the first full physical analysis, based on Imberts' RVs and  $u$ ,  $b$ ,  $v$ ,  $y$  photometry, was done by Clausen & Grønbech (1976). Later,

this photometric data set was reanalysed together with the new CORAVEL RVs by Andersen et al. (1989) who obtained the most up-to-date solution for UX Men. Comparison of this solution with our results is shown in Table 5.

Again, our results are, in general, in agreement with Andersen's. As for AI Phe, having eight RV measurements of UX Men, we succeeded to reach a better precision in the spectroscopic parameters

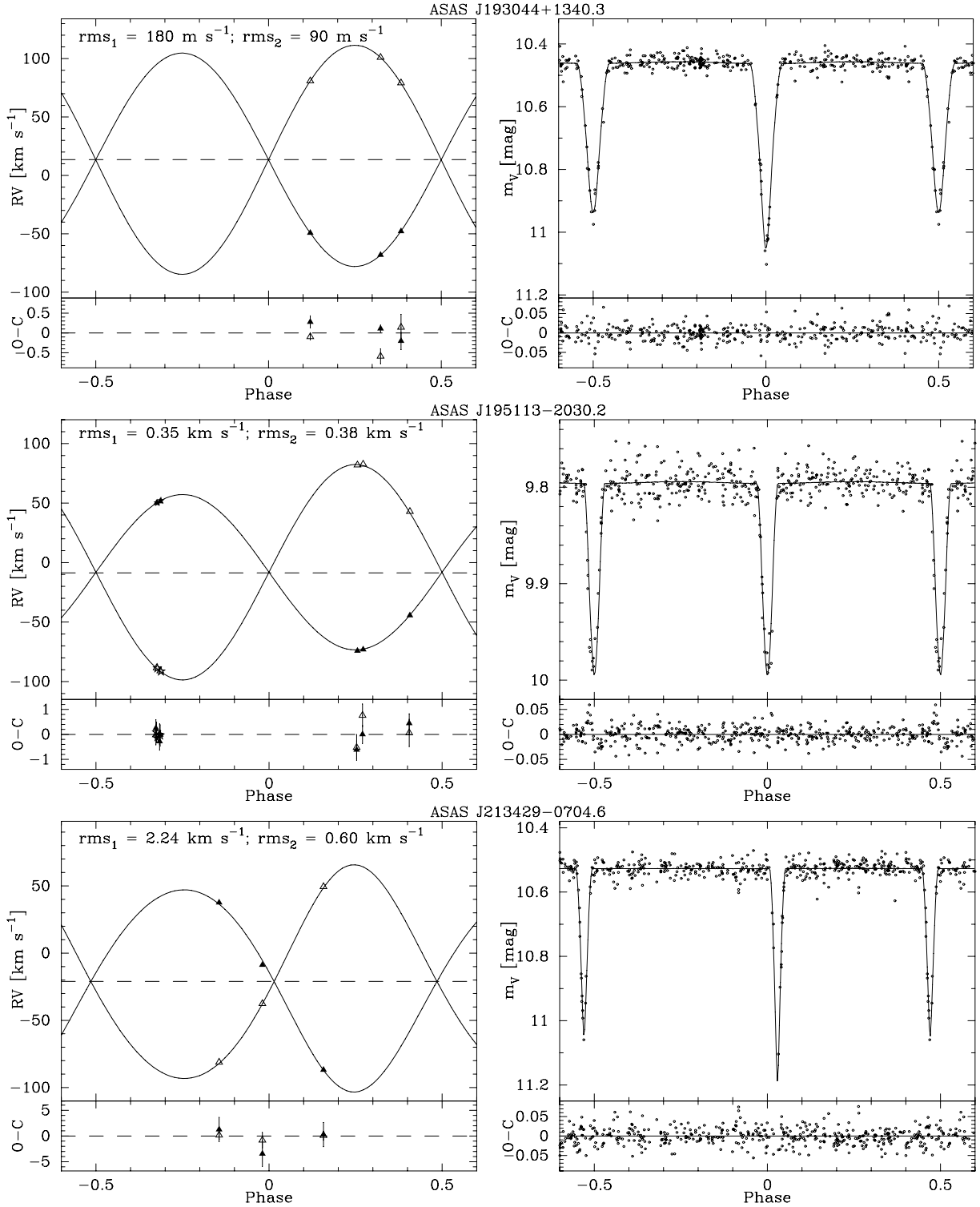


Figure 1 – continued

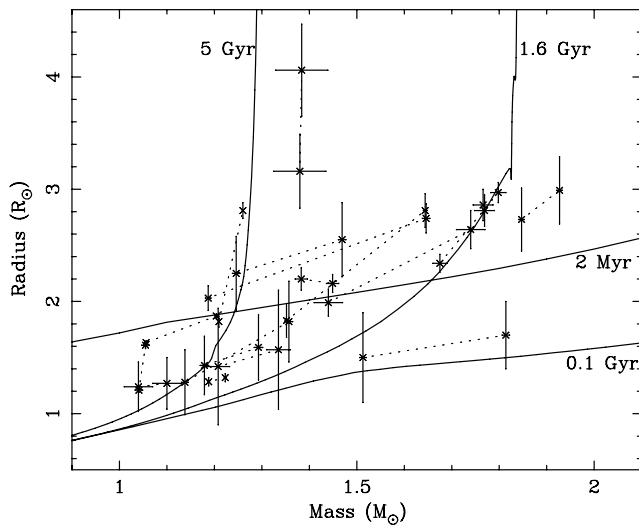
than Andersen et al. with 29 data points for the primary and 31 for the secondary. In our model, we fixed the eccentricity to 0. We found no significant improvement in the best-fitting model (in terms of rms) when  $e$  and  $\omega$  were set as free parameters and the resulting  $e$  was undistinguishable from 0 within the formal errors. The non-zero eccentricity may be however induced by a putative third body, found in NACO images by Tokovinin et al. (2006) about 0.751 arcsec from the binary.

### 5.3.3 ASAS J193044+1340.3 = V415 Aql

V415 Aql was first reported as a variable by Hoffmeister (1936). The first ephemeris  $2428670.532 + E \cdot 2.4628 \text{ d}$  was determined by Guthnick & Schneller (1936). The double-lined character was not previously reported, thus there was no RV curve obtained to date and the only known light curve analysis was done by Brancewicz & Dworak (1980) who derived an orbital period of 2.46 273 d. Our RV

**Table 3.** Phases of the primary and secondary minima of eight eccentric binaries, as given by PHOEBE.

ASAS ID	$\varphi_{\text{prim}}$	$\varphi_{\text{sec}}$
010934–4615.9	0.018 15	0.476 33
014616–0806.8	0.003 20	0.496 47
042041–0144.4	0.956 98	0.536 72
042724–2756.2	0.002 47	0.497 56
071626+0548.8	0.963 71	0.546 53
162637–5042.8	0.994 26	0.505 69
185512–0333.8	0.997 59	0.502 43
213429–0704.6	0.029 14	0.470 22

**Figure 2.** Masses and radii of 18 investigated systems with  $1\sigma$  uncertainties overplotted with the  $Y^2$  isochrones for solar metallicity and ages of 2 Myr, 0.1, 1.6 and 5.0 Gyr. Each isochrone is plotted as a solid line and labelled with its corresponding age. The components of the same pair are connected with thin dotted lines.

data, despite having only three measurements for every component, clearly show that the actual period is two times longer. This is confirmed by the ASAS light curve exhibiting unequal eclipses (see Fig. 1). If divided by 2, our period is in good agreement with the value from Brancewicz & Dworak (1980). Unfortunately, the uncertainties of their results are unavailable. In Table 6, we compare their results with ours. The improvement in the derived parameters is obvious. Also the distance estimate given by Brancewicz & Dworak (1980) (see Table 1) should be now treated with caution.

## 6 SUMMARY

Out of the 18 eclipsing binaries in our sample, 15 are new systems discovered by ASAS and fully characterized in this paper for the first time with the help of our RV measurements and ASAS photometry. Even though challenging seeing conditions during our observing runs at the AAT/UCLES prevented us from using the iodine technique for binary stars to the full extent of its capabilities (Konacki 2005; Konacki 2009), we were able to derive precise RVs for many of the binaries in our sample. In the best cases, when we were able to obtain useful spectra with the iodine cell, the precision of mass estimation is better than 1 per cent. In particular, in the case of AI Phe when we were able to apply the tomographic

**Table 4.** Comparison of our results for AI Phe with previous studies.

Parameter	Andersen et al. (1988)	Milone et al. (1992)	This paper
$P$ (d)		24.592 325(8)	24.592 41(8)
$K_1$ (km s $^{-1}$ )		50.95(8)	51.16(3)
$K_2$ (km s $^{-1}$ )		49.20(8)	49.11(2)
$v_\gamma$ (km s $^{-1}$ )		−1.84(4)	−0.750(12)
$q$		1.034(2)	1.0418(8)
$M_1 \sin^3 i$ ( $M_\odot$ )		1.194(4)	1.1922(10)
$M_2 \sin^3 i$ ( $M_\odot$ )		1.234(5)	1.2421(10)
$a$ (AU)	0.2225(2)	0.2223(3)	0.22 371(9)
$e$	0.1890(67)	0.1889(5)	0.187(4)
$\omega$ ( $^\circ$ )	109.60(67)	109.78(3)	110.1(9)
$i$ ( $^\circ$ )	88.45(3)	88.45(1)	84.4(5)
$M_1$ ( $M_\odot$ )	1.195(4)	1.190(6)	1.2095(11)
$M_2$ ( $M_\odot$ )	1.236(5)	1.231(5)	1.2600(11)
$R_1$ ( $R_\odot$ )	1.816(24)	1.762(7)	1.82(5)
$R_2$ ( $R_\odot$ )	2.930(48)	2.931(7)	2.81(7)
$T_2/T_1$	0.794(27)	0.816(31)	0.820(15)

**Table 5.** Comparison of our results for UX Men with previous studies.

Parameter	Andersen et al. (1989)	This paper
$P$ (d)	4.181 100(1)	4.181 096(3)
$K_1$ (km s $^{-1}$ )	87.41(25)	87.31(12)
$K_2$ (km s $^{-1}$ )	90.28(17)	89.90(8)
$v_\gamma$ (km s $^{-1}$ )	48.47(17)	48.86(5)
$q$	0.968(3)	0.9712(16)
$M_1 \sin^3 i$ ( $M_\odot$ )	1.238(6)	1.2229(15)
$M_2 \sin^3 i$ ( $M_\odot$ )	1.198(7)	1.1878(15)
$a$ ( $R_\odot$ )	14.678(25)	14.639(12)
$e \sin \omega$	0.0025(50)	0.0(fix)
$e \cos \omega$	0.000 83(7)	0.0(fix)
$i$ ( $^\circ$ )	89.6(1)	89.86(15)
$M_1$ ( $M_\odot$ )	1.238(6)	1.2229(15)
$M_2$ ( $M_\odot$ )	1.198(7)	1.1878(15)
$R_1$ ( $R_\odot$ )	1.348(13)	1.321(36)
$R_2$ ( $R_\odot$ )	1.274(13)	1.285(37)
$T_2/T_1$	0.993(32)	0.992(18)

**Table 6.** Comparison of our results for V415 Aql with previous studies.

Parameter	Brancewicz & Dworak (1980)	This paper
$P$ (d)	2.462 730	4.925 489(16)
$a$ ( $R_\odot$ )	11.60	18.44(8)
$R_1$ ( $R_\odot$ )	3.26	2.97(2)
$R_2$ ( $R_\odot$ )	4.05	2.82(8)
$T_2/T_1$	0.918	0.974(16)

disentangling of its composite spectra, the precision in  $M \sin^3 i$  is 0.08 per cent with just eight RV measurements for each component. This result can be improved by an order of magnitude with higher SNR spectra and millimagnitude photometry.

The iodine cell technique for double-lined and eclipsing binary stars (Konacki 2009) is no doubt a powerful tool for stellar astronomy. Its applications will provide new challenges not only for

the models of stellar structure and evolution but also for the techniques used to determine stellar metallicity. With masses and radii of stars accurate at the level of 0.01 per cent, it will be challenging to determine stellar metallicity with an adequate precision.

## ACKNOWLEDGMENTS

We would like to thank Dr Stephen Marsden from the Anglo-Australian Observatory and the AAO astronomers for their help during our observing runs on the AAT. We would like to thank Dr David Laney from the South African Astronomical Observatory for his help during our observing runs on the Radcliffe telescope.

This work is supported by the Foundation for Polish Science through a FOCUS grant and fellowship, by the Polish Ministry of Science and Higher Education through grants N203 005 32/0449 and 1P03D-021-29. The observations on the AAT/UCLES have been funded by the Optical Infrared Coordination network, a major international collaboration supported by the Research Infrastructures Programme of the European Commissions Sixth Framework Programme. This research has made use of the SIMBAD data base, operated at CDS, Strasbourg, France. This publication makes use of data products from the Two-Micron All Sky Survey (2MASS), which is a joint project of the University of Massachusetts and the Infrared Processing and Analysis Center/California Institute of Technology, funded by the National Aeronautics and Space Administration and the National Science Foundation.

## REFERENCES

- Andersen J., Clausen J. V., Gustaffson B., Nordstrom B., VandenBerg D. A., 1988, *A&A*, 196, 128
- Andersen J., Clausen J. V., Magain P., 1989, *A&A*, 211, 346
- Blake C. H., Torres G., Bloom J. S., Gaudi B. S., 2008, *ApJ*, 684, 635
- Brancewicz, H. K., Dworak T. Z., 1980, *AcA*, 30, 501
- Clausen J. V., Grønbech B., 1976, *A&A*, 48, 49
- Clausen J. V. et al., 2008, *A&A*, 487, 1095
- Cutri R. M. et al., 2003, The IRSA 2MASS All-Sky Catalog of Point Sources, NASA/IPAC Infrared Science Archive
- Etzel P. B., 1981, *Psbs. Conf.* 111
- Guthnick P., Schneller H., 1939, *Astron. Nachrichten*, 268, 165
- Hoffmeister C., 1936, *Astron. Nachrichten*, 225, 401
- Hrivnak B. J., Milone E. F., 1984, *ApJ*, 282, 748
- Imbert M., 1974, *A&A*, 32, 429
- Imbert M., 1979, *A&AS*, 36, 453
- Karami K., Mohebi R., 2007, *Chinese J. Astron. Astrophys.*, 7, 558
- Konacki M., 2005, *ApJ*, 626, 431
- Konacki M., 2009, in Pont F., Sasselov D., Holman M., eds, *Proc. IAU Symp. 253, Transiting Planets*. Cambridge Univ. Press, Cambridge, p. 141
- Kurucz R. L., 1992, in Barbury B., Renzini A., eds, *Proc. IAU Symp. 149, The Stellar Population of Galaxies*. Kluwert, Dordrecht, p. 225
- Lastennet E., Valls-Gabaud D., 2002, *A&A*, 396, 551
- Milone E. F., Hrivnak B. J., Clark T. A., Kjeldseth Moe O., Blades J. C., Shelton I., 1981, *IBVS*, 2060, 1
- Milone E. F., Stagg C. R., Kurucz R. L., 1992, *ApJS*, 79, 123
- Paczyński B., Szczygieł D. M., Pilecki B., Pojmański G., 2006, *MNRAS*, 368, 1311
- Perryman M. A. C. et al., 1997, *A&A*, 323, L49
- Pojmański G. 2002, *Acta Astron.*, 52, 397
- Popper D. M., Etzel P. B., 1981, *AJ*, 86, 102
- Prša A., Zwitter T., 2005, *ApJ*, 628, 426
- Prša A., 2006, *PHOEBE Scientific Reference*. University of Ljubljana, Ljubljana
- Southworth J., Maxted P. F. L., Smalley B., 2004a, *MNRAS*, 351, 1277
- Southworth J., Zucker S., Maxted P. F. L., Smalley B., 2004b, *MNRAS*, 355, 986
- Strohmeier W., 1972, *IBVS*, 610, 1
- Strohmeier W., Fischer H., Ott H., 1966, *IBVS*, 140, 1
- Tokunaga A. T., 2000, in Cox A. N., ed., *Allens' Astrophysical Quantities*, 4th edn. Springer-Verlag, New York, p. 143
- Tokovinin A., Thomas S., Sterzik M., Udry S., 2006, *A&A*, 450, 681
- Wilson R. E., Devinney E. J., 1971, *ApJ*, 166, 605
- Yi S., Demarque P., Kim Y.-C., Lee Y.-W., Ree C. H., Lejeune T., Barnes S., 2001, *ApJS*, 136, 417
- Zucker S., Mazeh T., 1994, *ApJ*, 420, 806

## APPENDIX A: ABSOLUTE RADIAL VELOCITY MEASUREMENTS

**Table A1.** Single, absolute RV measurements for all researched objects. Time of observation, final error, O – C and calibration method are given. ThAr-calibrated spectra are marked with ‘t’, and iodine-calibrated with ‘i’.

ASAS ID	BJD (2450000. +)	$v_1$ (km s <sup>-1</sup> )	$\sigma_{v_1}$ (km s <sup>-1</sup> )	O – C <sub>1</sub> (km s <sup>-1</sup> )	$v_2$ (km s <sup>-1</sup> )	$\sigma_{v_2}$ (km s <sup>-1</sup> )	O – C <sub>2</sub> (km s <sup>-1</sup> )	Calibration (t/i)
Systems observed with Radcliffe/GIRAFFE								
010538–8003.7	4007.4184	13.767	1.358	–0.369	–25.896	1.955	–0.244	t
	4008.5691	–48.402	1.309	0.215	34.786	2.094	–2.148	t
	4010.5241	–65.562	3.061	2.011	62.420	6.141	6.570	t
	4166.2696	54.048	2.553	2.579	–64.431	3.172	–1.571	t
174626–1153.0	3903.5470	51.205	1.810	–0.647	–147.011	2.830	0.258	t
	3903.5840	57.488	2.470	2.638	–151.550	3.080	–1.798	t
	3905.3660	–168.210	1.140	1.920	33.949	2.340	–1.846	t
	3906.3570	24.759	1.410	–0.074	–125.532	1.430	–0.507	t
Systems observed with AAT/UCLES								
014616–0806.8	4748.1195	–20.264	0.706	–1.541	95.132	0.322	0.444	i
	4748.1301	–20.239	0.719	–0.813	96.055	0.326	0.584	t
	4836.9694	–0.589	0.718	–0.688	74.374	0.346	0.674	t
	4836.9832	–1.255	0.706	–0.236	75.848	0.327	0.901	i
	4838.0049	–41.409	0.706	1.294	119.609	0.331	–1.786	i

Table A1 – *continued*

ASAS ID	BJD (2450000. +)	$v_1$ (km s <sup>-1</sup> )	$\sigma_{v_1}$ (km s <sup>-1</sup> )	O – C <sub>1</sub> (km s <sup>-1</sup> )	$v_2$ (km s <sup>-1</sup> )	$\sigma_{v_2}$ (km s <sup>-1</sup> )	O – C <sub>2</sub> (km s <sup>-1</sup> )	Calibration (t/i)
023631+1208.6	4727.1755	59.391	0.661	-0.605	-58.277	0.676	-0.438	t
	4748.1731	90.371	0.576	0.218	-93.688	0.453	0.076	t
	4837.0081	-59.088	1.178	0.921	86.165	0.593	1.012	t
	4838.0297	73.434	0.693	0.091	-73.876	0.940	-0.139	t
042041-0144.4	4839.9661	-71.914	0.815	-0.525	98.097	0.619	-0.627	t
	4727.2386	37.134	0.333	-0.149	-41.185	0.295	0.485	i
	4748.2447	-52.421	0.340	-0.330	56.302	0.307	-0.109	i
042724-2756.2	4837.0846	54.426	0.333	-0.022	-60.852	0.295	-0.357	i
	4838.1014	-13.658	0.334	0.453	14.537	0.301	-0.188	i
	4840.0839	-62.234	0.335	-0.016	67.706	0.299	0.182	i
	4748.2317	-46.626	0.092	0.018	92.797	0.102	0.017	i
071626+0548.8	4837.0945	-49.127	0.053	0.026	95.203	0.057	0.029	i
	4838.0716	-38.469	0.047	-0.082	84.879	0.049	-0.008	i
	4840.0494	53.716	0.077	0.101	-3.094	0.081	-0.091	i
	4837.1459	-29.687	0.209	-0.084	60.114	0.209	-0.030	i
085524-4411.3	4837.1565	-29.637	0.213	0.177	60.644	0.213	0.292	t
	4838.1523	-50.603	0.212	0.180	81.076	0.212	0.419	i
	4838.1628	-51.036	0.211	-0.476	80.916	0.218	0.125	t
	4840.1227	-13.610	0.217	-0.415	44.157	0.227	0.199	t
150145-524.2	4837.1658	88.902	0.153	-0.043	-55.966	0.187	-0.032	t
	4837.1788	88.908	0.106	-0.119	-55.867	0.161	0.162	i
	4838.2003	67.964	0.559	0.163	-31.948	0.949	-0.126	t
	4840.1752	-36.290	0.169	0.079	87.072	0.294	0.081	t
155259-6637.8	4840.1872	-37.096	0.134	-0.326	87.617	0.279	0.168	i
	4727.8800	-22.856	0.433	-0.017	31.536	0.404	-0.240	i
	4746.8978	-84.121	0.425	0.404	92.804	0.402	0.217	i
155358-5553.4	4747.8818	-49.147	0.417	-0.470	58.758	0.392	0.130	i
	4726.8822	-28.252	0.138	-0.075	43.217	0.053	0.064	i
	4747.8951	103.241	0.162	-0.182	-65.103	0.071	0.030	i
	4748.8874	66.360	0.148	0.076	-34.587	0.058	-0.040	i
162637-5024.8	4840.2618	99.190	0.240	0.265	-61.463	0.115	-0.063	i
	4725.8940	-53.747	0.245	-0.045	65.831	0.118	-0.039	i
	4726.8693	-84.018	0.123	0.342	97.428	0.058	-0.394	i
	4746.9343	89.580	0.162	-0.356	-83.583	0.076	0.356	i
185512-0333.8	4748.8984	-69.368	0.132	-0.101	82.366	0.064	0.241	i
	4725.9654	-5.360	0.052	0.697	-55.937	0.332	-0.912	t
	4726.9048	-48.709	0.054	-0.006	-4.294	0.337	0.406	t
	4727.9052	-83.688	0.046	-0.206	36.225	0.366	-0.115	t
193044+1340.3	4747.9195	-62.294	0.068	0.704	11.584	0.446	-0.582	t
	4724.9488	21.467	0.207	-0.935	-63.071	0.290	1.184	t
	4726.9390	-96.468	0.064	-0.207	78.198	0.183	0.152	t
	4746.9608	62.064	0.087	0.320	-111.946	0.122	-0.544	t
195113-2030.2	4726.9783	-49.255	0.155	0.277	80.940	0.084	-0.094	t
	4727.9801	-68.078	0.086	0.110	100.998	0.188	-0.588	t
	4747.9736	-47.881	0.216	-0.203	79.187	0.324	0.144	t
	4724.9114	-74.087	0.358	-0.617	82.055	0.516	-0.525	t
213429-0704.6	4725.0293	-72.957	0.367	0.001	82.638	0.461	0.761	t
	4725.9803	-44.384	0.378	0.445	42.941	0.546	0.061	t
	4727.9442	51.471	0.349	-0.281	-90.995	0.415	0.004	t
	4727.9567	52.053	0.169	0.003	-91.450	0.429	-0.040	i
010934-4615.9	4748.9997	50.112	0.345	0.248	-88.400	0.396	-0.019	t
	4749.0133	50.088	0.168	-0.149	-88.821	0.411	0.078	i
	4726.0762	-8.783	2.483	-3.445	-37.554	1.499	-0.818	t
Systems observed with AAT/UCLES with tomographically disentangled spectra	4727.0779	-86.844	2.353	0.271	49.419	0.859	0.087	t
	4748.0581	37.655	2.359	1.261	-81.116	0.860	0.172	t
	4726.1839	-50.010	0.067	0.039	46.563	0.032	-0.005	i
010934-4615.9	4727.1199	-54.702	0.065	0.008	51.034	0.030	-0.012	i
	4728.1348	-54.588	0.068	-0.082	50.879	0.032	0.029	i
	4748.1047	-10.478	0.065	0.042	8.647	0.031	0.037	i
	4749.1254	-29.290	0.068	-0.095	26.506	0.036	-0.034	i

Table A1 – *continued*

ASAS ID	BJD (2450000. +)	$v_1$ (km s <sup>-1</sup> )	$\sigma_{v_1}$ (km s <sup>-1</sup> )	$O - C_1$ (km s <sup>-1</sup> )	$v_2$ (km s <sup>-1</sup> )	$\sigma_{v_2}$ (km s <sup>-1</sup> )	$O - C_2$ (km s <sup>-1</sup> )	Calibration (t/i)
	4836.9479	30.615	0.066	0.032	-30.809	0.031	0.023	i
	4837.9913	37.186	0.067	-0.067	-37.231	0.029	0.000	i
	4839.9391	45.639	0.064	-0.051	-45.336	0.029	-0.009	i
053003–7614.9	4726.2312	10.474	0.186	0.089	88.834	0.132	-0.112	i
	4727.2714	126.622	0.182	-0.284	-31.545	0.137	0.028	i
	4747.2639	25.567	0.186	-0.128	72.924	0.141	-0.196	i
	4748.2774	131.771	0.201	-0.388	-36.657	0.130	0.492	i
	4837.1270	75.675	0.180	-0.124	21.225	0.125	0.178	i
	4838.1106	-31.653	0.180	-0.027	131.483	0.125	-0.060	i
	4838.1334	-32.599	0.181	0.104	132.385	0.125	0.391	i
	4840.0952	122.517	0.183	-0.190	-26.918	0.136	-0.107	i

This paper has been typeset from a  $\text{\TeX}/\text{\LaTeX}$  file prepared by the author.